Draft version May 29, 2019
Typeset using LaTeX **twocolumn** style in AASTeX62

TESS ASTEROSEISMOLOGY OF THE KNOWN RED-GIANT HOST STARS HD 212771 AND HD 203949

Tiago L. Campante,[1,2,3] Enrico Corsaro,[4] Mikkel N. Lund,[5] Benoît Mosser,[6] Aldo Serenelli,[7,8] Dimitri Veras,[9,10,*] Vardan Adibekyan,[1] Hormazad M. Antia,[11] Warrick Ball,[12,5] Sarbani Basu,[13] Timothy R. Bedding,[14,5] Diego Bossini,[1] Guy R. Davies,[12,5] Rafael A. García,[15,16] Rasmus Handberg,[5] Marc Hon,[17] Stephen R. Kane,[18] Steven D. Kawaler,[19] James S. Kuszlewicz,[20,5] Miles Lucas,[19] Savita Mathur,[21,22] Martin B. Nielsen,[12,5] Sabine Reffert,[23] Víctor Silva Aguirre,[5] Keivan G. Stassun,[24,25] Dennis Stello,[17,14,5] Stephan Stock,[23] Mathieu Vrard,[1] Mutlu Yildiz,[26] William J. Chaplin,[12,5] Daniel Huber,[27] Jacob L. Bean,[28] Zeynep Çelik Orhan,[26] Margarida S. Cunha,[1,2] Jørgen Christensen-Dalsgaard,[5] Hans Kjeldsen,[5] Travis S. Metcalfe,[29,20] Andrea Miglio,[12,5] Mário J. P. F. G. Monteiro,[1,2] Benard Nsamba,[1] Sibel Örtel,[26] Joshua Pepper,[30] Filipe Pereira,[1] Sérgio G. Sousa,[1,2] Maria Tsantaki,[1] and Margaret C. Turnbull[31]

[1] *Instituto de Astrofísica e Ciências do Espaço, Universidade do Porto, Rua das Estrelas, 4150-762 Porto, Portugal*
[2] *Departamento de Física e Astronomia, Faculdade de Ciências da Universidade do Porto, Rua do Campo Alegre, s/n, 4169-007 Porto, Portugal*
[3] *Kavli Institute for Theoretical Physics, University of California, Santa Barbara, CA 93106-4030, USA*
[4] *INAF — Osservatorio Astrofisico di Catania, via S. Sofia 78, 95123 Catania, Italy*
[5] *Stellar Astrophysics Centre (SAC), Department of Physics and Astronomy, Aarhus University, Ny Munkegade 120, 8000 Aarhus C, Denmark*
[6] *LESIA, Observatoire de Paris, PSL Research University, CNRS, Sorbonne Université, Université Paris Diderot, 92195 Meudon, France*
[7] *Institute of Space Sciences (ICE, CSIC) Campus UAB, Carrer de Can Magrans, s/n, E-08193, Bellaterra, Spain*
[8] *Institut d'Estudis Espacials de Catalunya (IEEC), C/Gran Capità, 2-4, E-08034, Barcelona, Spain*
[9] *Centre for Exoplanets and Habitability, University of Warwick, Coventry CV4 7AL, UK*
[10] *Department of Physics, University of Warwick, Coventry CV4 7AL, UK*
[11] *Tata Institute of Fundamental Research, Mumbai, India*
[12] *School of Physics and Astronomy, University of Birmingham, Edgbaston, Birmingham B15 2TT, UK*
[13] *Department of Astronomy, Yale University, P.O. Box 208101, New Haven, CT 06520-8101, USA*
[14] *Sydney Institute for Astronomy (SIfA), School of Physics, University of Sydney, NSW 2006, Australia*
[15] *IRFU, CEA, Université Paris-Saclay, F-91191 Gif-sur-Yvette, France*
[16] *AIM, CEA, CNRS, Université Paris-Saclay, Université Paris Diderot, Sorbonne Paris Cité, F-91191 Gif-sur-Yvette, France*
[17] *School of Physics, The University of New South Wales, Sydney NSW 2052, Australia*
[18] *Department of Earth and Planetary Sciences, University of California, Riverside, CA 92521, USA*
[19] *Department of Physics and Astronomy, Iowa State University, Ames, IA 50011, USA*
[20] *Max-Planck-Institut für Sonnensystemforschung, Justus-von-Liebig-Weg 3, 37077 Göttingen, Germany*
[21] *Instituto de Astrofísica de Canarias (IAC), E-38205 La Laguna, Tenerife, Spain*
[22] *Universidad de La Laguna (ULL), Departamento de Astrofísica, E-38206 La Laguna, Tenerife, Spain*
[23] *Landessternwarte, Zentrum für Astronomie der Universität Heidelberg, Königstuhl 12, 69117 Heidelberg, Germany*
[24] *Vanderbilt University, Department of Physics and Astronomy, 6301 Stevenson Center Ln., Nashville, TN 37235, USA*
[25] *Vanderbilt Initiative in Data-intensive Astrophysics (VIDA), 6301 Stevenson Center Ln., Nashville, TN 37235, USA*
[26] *Department of Astronomy and Space Sciences, Science Faculty, Ege University, 35100, Bornova, İzmir, Turkey*
[27] *Institute for Astronomy, University of Hawai'i, 2680 Woodlawn Drive, Honolulu, HI 96822, USA*
[28] *Department of Astronomy and Astrophysics, University of Chicago, 5640 S. Ellis Avenue, Chicago, IL 60637, USA*
[29] *Space Science Institute, 4750 Walnut Street, Suite 205, Boulder, CO 80301, USA*
[30] *Department of Physics, Lehigh University, 16 Memorial Drive East, Bethlehem, PA 18015, USA*
[31] *SETI Institute, Carl Sagan Center for the Study of Life in the Universe, Off-Site: 2801 Shefford Drive, Madison, WI 53719, USA*

(Received January 1, 2018; Revised January 7, 2018; Accepted May 29, 2019)

Submitted to ApJ

Corresponding author: Tiago L. Campante
tiago.campante@astro.up.pt

ABSTRACT

The *Transiting Exoplanet Survey Satellite* (TESS) is performing a near all-sky survey for planets that transit bright stars. In addition, its excellent photometric precision enables asteroseismology of solar-type and red-giant stars, which exhibit convection-driven, solar-like oscillations. Simulations predict that TESS will detect solar-like oscillations in nearly 100 stars previously known to host planets. In this paper, we present the asteroseismic analysis of the evolved known hosts HD 212771 and HD 203949 (a red-giant branch and a red-clump star, respectively), both systems having a long-period planet detected through radial velocities. This is the first detection of oscillations in any known exoplanet-host star by TESS, further showcasing the mission's potential to conduct asteroseismology of red-giant stars. We estimate the fundamental properties of both stars through a grid-based modeling approach that uses global asteroseismic parameters as input. Noting the large discrepancy between HD 203949's asteroseismic mass ($M_* = 1.00 \pm 0.16\,\mathrm{M}_\odot$) and the mass quoted in the discovery paper ($M_* = 2.1 \pm 0.1\,\mathrm{M}_\odot$), we investigate the planet's past orbital evolution and discuss how it could have avoided engulfment at the tip of the red-giant branch. Finally, HD 212771 was observed by K2 during its Campaign 3, thus allowing for a preliminary comparison of the asteroseismic performances of TESS and K2. We estimate the ratio of the observed oscillation amplitudes for this star to be $A_{\rm max}^{\rm TESS}/A_{\rm max}^{\rm K2} = 0.75 \pm 0.14$, consistent with the expected ratio of ~ 0.85 due to TESS's redder bandpass.

Keywords: asteroseismology — planet-star interactions — stars: fundamental parameters — stars: individual (HD 212771, HD 203949) — techniques: photometric

1. INTRODUCTION

Major advances in stellar interiors physics and evolution have recently been made possible by asteroseismology. This has largely been due to the exquisite space-based data made available by CNES/ESA's CoRoT (Baglin et al. 2009) and NASA's *Kepler*/K2 (Borucki et al. 2010; Howell et al. 2014) missions. In particular, asteroseismology has vastly benefited the study of solar-type and red-giant stars, which exhibit convection-driven, solar-like oscillations (for a review, see Chaplin & Miglio 2013). The revolution triggered by CoRoT and *Kepler*/K2 is set to continue over the coming decade, with NASA's TESS (Ricker et al. 2015) and ESA's PLATO (Rauer et al. 2014) missions expected to raise the number of known solar-like oscillators by up to two orders of magnitude (Huber 2018).

Fueled by the wealth of high-quality seismic data, the past few years have witnessed an ever-growing effort being devoted to the development of novel techniques for the estimation of fundamental stellar properties. The focus has been placed on uniform data analysis (e.g., Davies et al. 2016; Lund et al. 2017b) and stellar modeling (e.g., Serenelli et al. 2017; Silva Aguirre et al. 2017; Nsamba et al. 2018) strategies, as well as on state-of-the-art optimization procedures that make use of individual oscillation frequencies (e.g., Metcalfe et al. 2010; Silva Aguirre et al. 2015; Rendle et al. 2019).

These techniques make it possible to estimate precise properties of large numbers of field stars, for which such information is sparse. As a result, asteroseismology is having a profound impact on modern astrophysics, notably on the field of exoplanetary science (Campante et al. 2018). Characterization of exoplanet-host stars via asteroseismology allows for unmatched precision in the absolute properties of their planets (Huber et al. 2013a; Ballard et al. 2014; Campante et al. 2015; Silva Aguirre et al. 2015; Lundkvist et al. 2016). Furthermore, asteroseismology enables constraints on the spin-orbit alignment of exoplanet systems (Chaplin et al. 2013; Huber et al. 2013b; Campante et al. 2016a; Kamiaka et al. 2019) as well as statistical inferences on orbital eccentricities via asterodensity profiling (Sliski & Kipping 2014; Van Eylen & Albrecht 2015; Van Eylen et al. 2019).

The *Transiting Exoplanet Survey Satellite* (TESS) is performing a near all-sky survey for planets that transit bright stars. Moreover, its excellent photometric precision, combined with its fine time sampling and long intervals of uninterrupted observations, enables asteroseismology of solar-type and red-giant stars (Campante et al. 2016b; Schofield et al. 2019). In particular, simulations predict that TESS will detect solar-like oscillations in nearly 100 solar-type and red-giant stars previously known to host planets (Campante et al. 2016b).

In this paper, we present the asteroseismic analysis of the evolved known hosts HD 212771 and HD 203949, both systems having a long-period planet detected through the radial-velocity (RV) method. This is the first detection of oscillations in any known exoplanet-

* STFC Ernest Rutherford Fellow

host star by TESS and follows the discovery of the first planet transiting a star in which oscillations could be measured (TOI-197 or TESS Object of Interest 197; Huber et al. 2019).

HD 212771 (TIC 12723961, HIP 110813) is a bright (with apparent TESS magnitude $T = 6.753$), spectroscopically-classified subgiant (G8 IV; Houk & Smith-Moore 1988), being among the targets of the RV planet survey of Johnson et al. (2007). It hosts a Jovian planet with minimum mass $M_{\rm p} \sin i = 2.3 \pm 0.4\,M_{\rm J}$ in a 373.3-day orbit (Johnson et al. 2010). HD 212771 was subsequently observed by K2 in short cadence during its Campaign 3, spanning a total of $\sim$69 days. This allowed estimation of its fundamental properties through a grid-based modeling approach that used global asteroseismic parameters, complementary spectroscopy and a parallax-based luminosity as input (Campante et al. 2017; North et al. 2017).

HD 203949 (TIC 129649472, HIP 105854) is a bright ($T = 4.753$) horizontal-branch star (K2 III; Houk 1982). A massive planet ($M_{\rm p} \sin i = 8.2 \pm 0.2\,M_{\rm J}$) was discovered in a 184.2-day orbit around HD 203949 by Jones et al. (2014) as part of the EXoPlanets aRound Evolved StarS (EXPRESS) project (Jones et al. 2011).

The rest of this paper is organized as follows. In Sect. 2, we present the available observational data (including the TESS photometry). This is followed by an asteroseismic analysis (Sect. 3) and the estimation of fundamental stellar properties through a grid-based modeling approach (Sect. 4). Finally, we discuss our results in Sect. 5 and provide an outlook in Sect. 6.

2. OBSERVATIONS

2.1. *TESS Photometry*

TESS observed HD 212771 and HD 203949 in 2-minute cadence over 27.4 days during Sectors 2 and 1 of Cycle 1, respectively. Both targets were part of a larger cohort of 79 "fast-track" targets that were processed using a special version (Handberg & Lund 2018) of the TESS Asteroseismic Science Operations Center[1] (TASOC; Lund et al. 2017a) photometry pipeline[2]. Starting from calibrated target pixel files, aperture photometry was conducted following a procedure similar to the one adopted in the `K2P`[2] pipeline (Lund et al. 2015), originally developed to generate light curves from data collected by K2. The extracted light curves were subsequently corrected for systematic effects using the KASOC filter (Handberg & Lund 2014).

Figure 1 shows the light curves of HD 212771 (left panel) and HD 203949 (right panel) produced by the TASOC pipeline. Both light curves have high duty cycles ($\sim$98 % and $\sim$94 %, respectively), displaying a gap midway through (due to the data downlink) that separates the two spacecraft orbits in each sector. A 2.5-day periodicity can be seen, especially in the bottom left subpanel, caused by the spacecraft's angular momentum dumping cycle. Moreover, a region of large jitter can be seen in the right panel towards the end of the sector, a feature common to Sector 1 pointings (Handberg & Lund 2018).

2.2. *High-Resolution Spectroscopy*

We adopt the atmospheric parameters and elemental abundances obtained for HD 212771 by Campante et al. (2017), which are based on the analysis of a high-quality FEROS spectrum (see Table 1).

Particular care must, however, be taken regarding HD 203949, since use of the model-independent scaling relation $g \propto \nu_{\rm max}\, T_{\rm eff}^{1/2}$ (Brown et al. 1991; Kjeldsen & Bedding 1995; Belkacem et al. 2011), where $\nu_{\rm max}$ is the frequency of maximum oscillation amplitude (see Sect. 3.1), leads to an initial estimate of the surface gravity that significantly underestimates the spectroscopic value quoted in the discovery paper ($\log g = 2.94 \pm 0.20$; Jones et al. 2011, 2014). This discrepancy is confirmed by applying the Bayesian inference method of Stock et al. (2018), originally developed to determine the stellar parameters of the K-giant sample observed by the Lick planet search, and which returns $\log g \sim 2.34$.

Therefore, we instead adopt the spectroscopic parameters listed for HD 203949 in the SWEET-Cat catalog[3] (Santos et al. 2013), whose $\log g$ is compatible with the one predicted from asteroseismology. These are based on the analysis of a high-resolution ($R \sim 100{,}000$) UVES spectrum (for details, see Sousa et al. 2018) and are listed in Table 2. Analysis of a lower-resolution ($R \sim 48{,}000$) FEROS spectrum by the same authors, albeit considering a larger number of iron lines, led to fully consistent spectroscopic parameters.

We further conducted a detailed abundance analysis of HD 203949 based on both the UVES and FEROS spectra, following the methodology described in Adibekyan et al. (2012, 2015a). Abundances derived from the two spectra are consistent within 1σ, with UVES-based results being slightly more precise. Our analysis shows that HD 203949 has a chemical composition typical of a thin-disk, metal-rich K giant (e.g., Adibekyan et al. 2015b; Jofré et al. 2015). The star shows enhancement

[1] https://tasoc.dk/
[2] https://github.com/tasoc
[3] https://www.astro.up.pt/resources/sweet-cat/

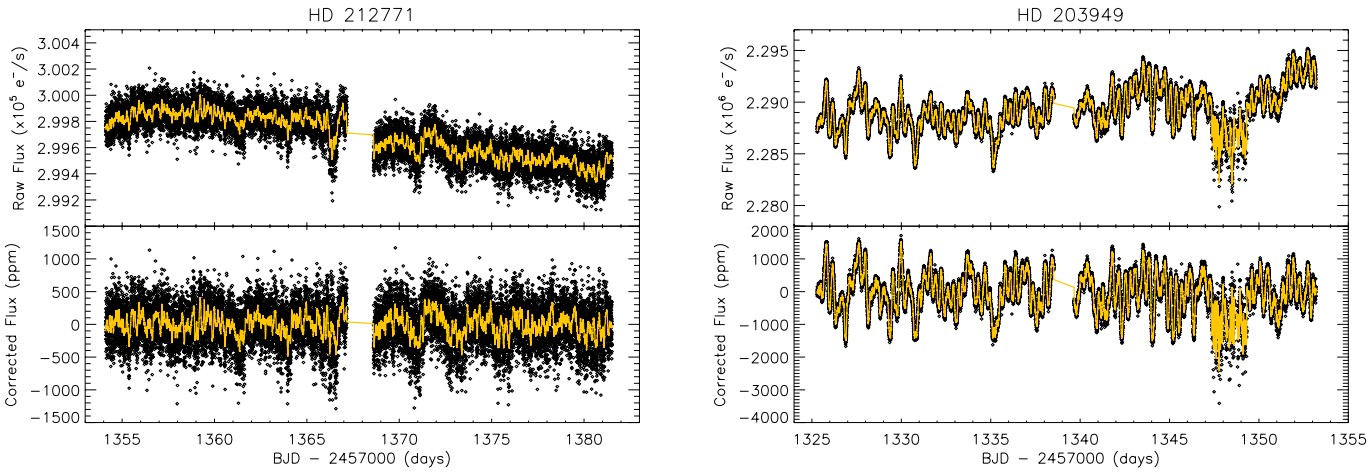

Figure 1. Light curves of HD 212771 (left panel) and HD 203949 (right panel) produced by the TASOC photometry pipeline. In each panel, raw (top) and corrected (bottom) 2-minute cadence light curves are displayed. A smoothed — using a 1-hour (HD 212771) and 10-minute (HD 203949) boxcar filter — version of the light curve is depicted by a yellow curve in each subpanel.

in Na and Al relative to iron ([Na/Fe] $= 0.22 \pm 0.13$ dex and [Al/Fe] $= 0.25 \pm 0.12$ dex based on the UVES spectrum), typical of evolved stars (e.g., Adibekyan et al. 2015b). Finally, we computed the relative abundance of α elements as the unweighted mean of the Mg, Si, Ca and Ti abundances derived from the UVES spectrum, resulting in [α/Fe] $= 0.07 \pm 0.09$ dex.

2.3. *Broadband Photometric Spectral Energy Distribution*

We fitted the spectral energy distributions (SEDs) of both stars using broadband photometry to determine empirical constraints on the stellar radii and luminosities, following the method described in Stassun & Torres (2016) and Stassun et al. (2018a). The available broadband photometry in published all-sky catalogs (i.e., APASS, 2MASS and WISE) provides coverage over the wavelength range $\approx$0.4–22 μm. For each star, we fitted a standard Kurucz (2013) stellar atmosphere model, selected according to the spectroscopically-determined $T_{\rm eff}$, $\log g$ and [Fe/H] (see Sect. 2.2). With these constraints fixed, the remaining free parameter in the fit is the extinction, A_V, which we limited to the maximum for the line of sight from the dust maps of Schlegel et al. (1998). Finally, we integrated the (non-reddened) SED to obtain the bolometric flux at Earth ($F_{\rm bol}$) which, with the $T_{\rm eff}$ and the *Gaia* DR2 distance (adjusted for the systematic offset of Stassun & Torres 2018), gives the stellar radius.

The best-fit parameters for HD 212771, with reduced $\chi^2 = 4.7$, are: $A_V = 0.04 \pm 0.04$, $F_{\rm bol} = (3.06 \pm 0.14) \times 10^{-8}$ erg s^{-1} cm^{-2}, resulting in $R_\star = 4.44 \pm 0.13$ R$_\odot$ and $L_\star = 11.67 \pm 0.57$ L$_\odot$. For HD 203949, the best-fit parameters, with reduced $\chi^2 = 3.7$, are: $A_V = 0.13 \pm 0.10$, $F_{\rm bol} = (2.27 \pm 0.22) \times 10^{-7}$ erg s^{-1} cm^{-2}, resulting in $R_\star = 10.30 \pm 0.51$ R$_\odot$ and $L_\star = 43.34 \pm 4.27$ L$_\odot$.

3. ASTEROSEISMOLOGY

Figures 2 and 3 show the power spectra of HD 212771 and HD 203949, respectively, computed based on the TASOC light curves. These reveal a clear power excess due to solar-like oscillations at $\sim 230\,\mu$Hz and $\sim 30\,\mu$Hz, respectively.

3.1. *Global Oscillation Parameters*

The large frequency separation, $\Delta\nu$, and frequency of maximum oscillation amplitude, $\nu_{\rm max}$, were measured based on the analysis of the above power spectra. A range of well-tested and complementary automated methods were used in the analysis (Huber et al. 2009, 2011; Mosser & Appourchaux 2009; Mathur et al. 2010; Mosser et al. 2011; Corsaro & De Ridder 2014; Corsaro et al. 2015; Davies & Miglio 2016; Campante 2018; Yu et al. 2018), which have previously been extensively applied to data from *Kepler*/K2 (e.g., Hekker et al. 2011; Verner et al. 2011). Returned values were subject to a preliminary step which involved the rejection of outliers following Peirce's criterion (Peirce 1852; Gould 1855). For each star, we finally adopt the values of $\Delta\nu$ and $\nu_{\rm max}$ corresponding to the smallest normalized root-mean-square deviation about the median, considering both parameters simultaneously (i.e., both parameters originate from the same source/method). Uncertainties are recalculated by adding in quadrature the corresponding formal uncertainty and the standard deviation of the parameter estimates returned by all methods. Consolidated values for $\Delta\nu$ and $\nu_{\rm max}$ are given in Tables 1 and 2.

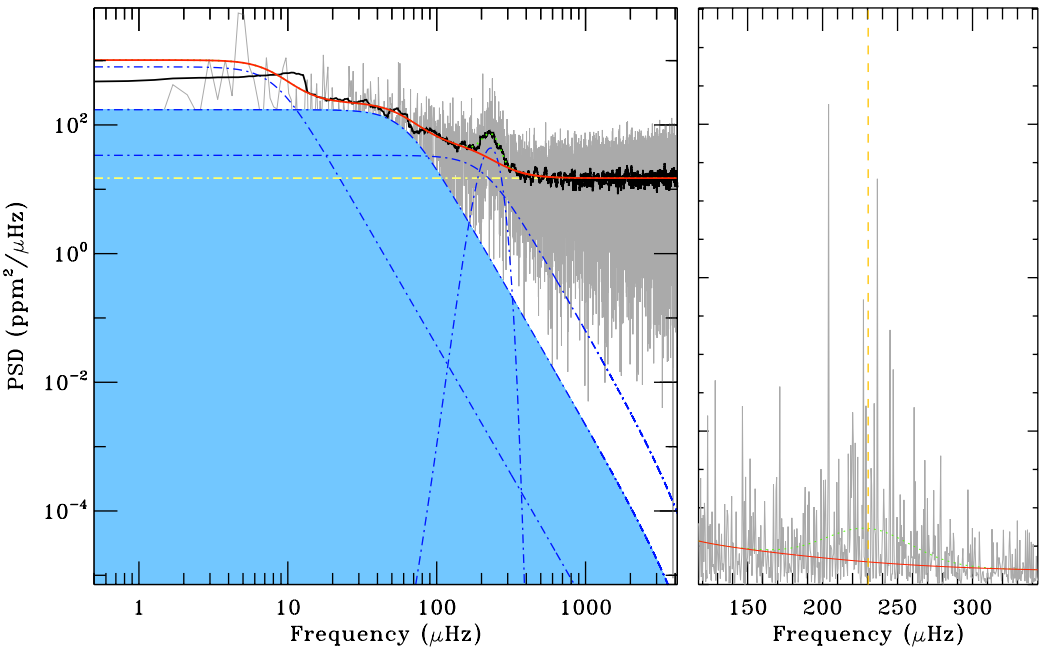

Figure 2. *Left Panel:* Power spectral density (PSD) of HD 212771. The PSD is shown in gray (with a heavily smoothed version in black). The solid red curve is a global fit to the background, consisting of three Harvey-like profiles (blue dot-dashed curves) plus white noise (yellow horizontal dot-dashed line). A global fit to the background and oscillation power excess (blue dot-dashed Gaussian curve) is visible at $\sim 230\,\mu$Hz as a dotted green curve. *Right Panel:* Blowup of the oscillation power excess. The orange vertical dashed line is a proxy for $\nu_{\rm max}$.

3.2. *HD 212771: Asymptotic Mixed-Mode Pattern and Rotation*

Mixed modes in HD 212771 were analyzed following the method of Mosser et al. (2015), which revealed the signature of the period spacing, $\Delta\Pi_1$. Its value, computed as in Vrard et al. (2016), is $\Delta\Pi_1 = 84.3 \pm 1.6$ s. A fit of the mixed-mode pattern provides a more refined value of the period spacing, $\Delta\Pi_1 = 85.3 \pm 0.3$ s, and a coupling factor $q = 0.19 \pm 0.03$. Such values are in agreement with the general trends found in *Kepler* data for stars on the red-giant branch (Mosser et al. 2017). This is supported by the star's location in a $\Delta\Pi_1$ – $\Delta\nu$ diagram (see fig. 1 of Mosser et al. 2014). We thus reclassify HD 212771 as a low-luminosity red-giant branch (LLRGB) star based on asteroseismology.

Since the mixed-mode pattern also revealed rotational multiplets, we next performed an analysis of the rotational splittings of dipole mixed modes (based on a power spectrum oversampled by a factor of 4). In a preliminary step, rotational splittings were identified using an asymptotic mixed-mode pattern modulated by a core rotation rate of 400 nHz. Comparison of the spectrum with the asymptotic fit revealed 13 mixed modes with a height-to-background ratio larger than five, among which 8 are forming rotational doublets, corresponding to the mixed-mode orders −40, −38, −35, and −34 (see Table 3). The remaining components are identified as being $|m| = 1$ modes. The absence of any significant dipole mode with azimuthal order $m = 0$ is in favor of a star seen edge-on. As shown by Kamiaka et al. (2018), deriving a reliable and precise value of the stellar inclination is difficult when the height-to-background ratio of the modes is small. Based on the observed height-to-background ratio of the rotational doublets, an inclination angle larger than 75° is to be expected, consistent with an aligned transiting system.

To derive the mean core rotation, rotational splittings are expressed as a function of ζ, which describes the relative contribution of the inner radiative region to the mode inertia (Goupil et al. 2013; Deheuvels et al. 2014; Mosser et al. 2018). This method allows us to derive the individual splitting of each component of the multiplet, with the total rotational splitting between the $m = -1$ and $m = +1$ components being split according to the respective ζ coefficients of each mode. We further assume that the uncertainties of the unresolved dipole mixed modes cannot be less than half the frequency resolution. The method then returns a nominal, albeit imprecise, mean core rotation of $\delta\nu_{\rm rot} = 354 \pm 151$ nHz.

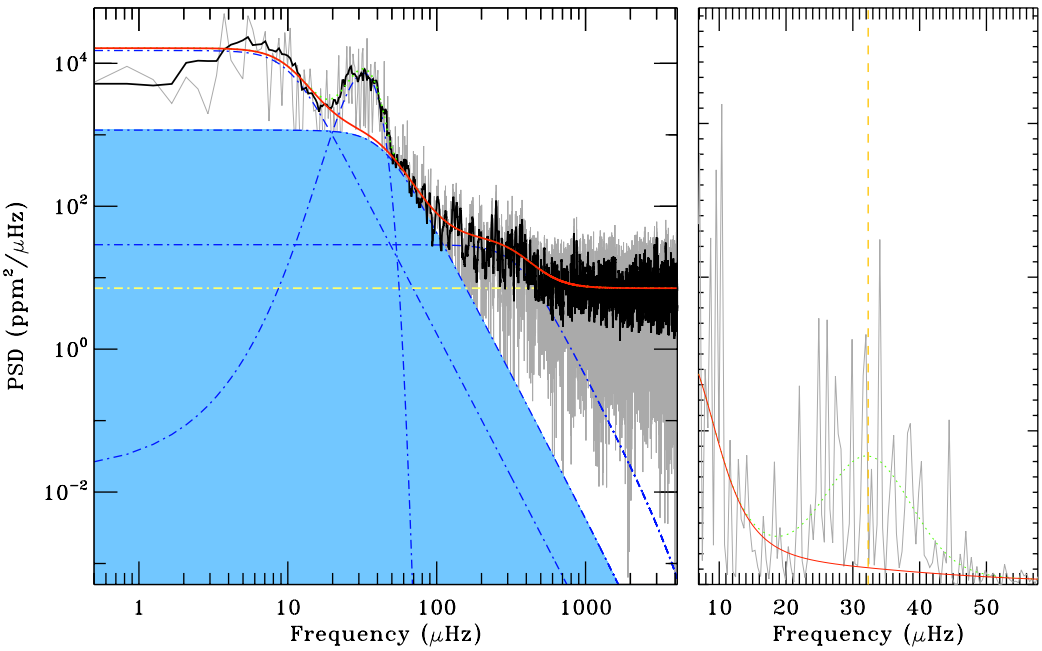

Figure 3. *Left Panel:* Power spectral density (PSD) of HD 203949. The PSD is shown in gray (with a heavily smoothed version in black). The solid red curve is a global fit to the background, consisting of three Harvey-like profiles (blue dot-dashed curves) plus white noise (yellow horizontal dot-dashed line). A global fit to the background and oscillation power excess (blue dot-dashed Gaussian curve) is visible at $\sim 30\,\mu$Hz as a dotted green curve. *Right Panel:* Blowup of the oscillation power excess. The orange vertical dashed line is a proxy for $\nu_{\rm max}$.

3.3. *HD 203949: Evolutionary State and a Second Power Excess*

Red-clump (RC) stars, i.e., cool helium-core burning stars, occupy a confined parameter space in the $\Delta\Pi_1$ – $\Delta\nu$ diagram around 300 s and 4.1 μHz (Mosser et al. 2012). Although the $\Delta\nu$ value measured for HD 203949 is consistent with it being an RC star, the low frequency resolution of the power spectrum hinders a measurement of $\Delta\Pi_1$. This in turn prevents a definite classification of its evolutionary state from being made based on the $\Delta\Pi_1$ – $\Delta\nu$ diagram, due to the underlying degeneracy for $\Delta\nu \lessapprox 10\mu$Hz (e.g., Mosser et al. 2014). Alternatively, we applied the asteroseismic deep learning method of Hon et al. (2017, 2018), which efficiently classifies the evolutionary state of oscillating red giants by recognizing visual features in their asteroseismic power spectra. Application of this method to the power spectrum of HD 203949 returns a probability of it being an RC star of $p = 0.98 \pm 0.01$, and we hereafter take this as an unambiguous classification of its evolutionary state.

For HD 203949 we find that, in order to properly fit the background PSD, three Harvey-like profiles must be included. One of these profiles, however, has a timescale and amplitude that do not conform with expectations based on the measured $\nu_{\rm max}$ (e.g., Kallinger et al. 2014), with a "knee" at $\sim 300\mu$Hz (see Fig. 3). We suspect that this second power hump is caused by a jitter in the TESS data that remains after applying the KASOC filter. We note that the power hump is also evident from the simple aperture photometry (SAP) delivered by the TESS Science Processing Operations Center (SPOC; Jenkins et al. 2016), while it is largely removed in the co-trended Presearch Data Conditioning SAP (PDCSAP) — the oscillation signal in the PDCSAP data is, however, of lesser quality than the one present in the TASOC data.

Support for the hypothesis of a jitter causing the second power hump comes from the `MOM_CENTR2` data delivered by SPOC, which gives the flux-centroid along rows on the CCD. The PSD of this centroid time series shows a clear excess at $\sim 300\,\mu$Hz. A jitter at this frequency would cause a variation in the flux from inter/intra pixel sensitivity and from flux exiting/entering the aperture. We find that adopting a larger aperture than the one set by the TASOC pipeline makes the power hump disappear, but at the cost of a degraded oscillation signal. As the power hump is well separated in frequency from the power excess due to oscillations, we can account for it in the fitted background without affecting the analysis of the oscillations.

Table 1. Stellar Parameters (HD 212771)

Parameter	Value	Source
Basic Properties		
TIC	12723961	1
Hipparcos ID	110813	2
TESS Mag.	6.753	1
Sp. Type	G8 IV	3
Spectroscopy		
$T_{\rm eff}$ (K)	5065 ± 75	4
[Fe/H] (dex)	-0.10 ± 0.10	4
[α/Fe] (dex)	0.06 ± 0.05[a]	4
$\log g_{\rm spec}$ (cgs)	3.37 ± 0.17	4
SED & *Gaia* DR2 Parallax		
π (mas)	9.0498 ± 0.0548[b]	5
$R_{*,\rm SED}$ ($R_\odot$)	4.44 ± 0.13	6
L_* ($L_\odot$)	11.67 ± 0.57	6
Asteroseismology		
M_* ($M_\odot$)	1.42 ± 0.07	6
R_* ($R_\odot$)	4.61 ± 0.09	6
ρ_* (gcc)	0.02048 ± 0.00050	6
$\log g$ (cgs)	3.263 ± 0.010	6
t (Gyr)	2.90 ± 0.47	6
$\Delta\nu$ (μHz)	16.25 ± 0.19	6
$\nu_{\rm max}$ (μHz)	226.6 ± 9.4	6
$\Delta\Pi_1$ (s)	85.3 ± 0.3	6

[a] The uncertainty (0.02) reported in (4) is not correct.

[b] Adjusted for the systematic offset of Stassun & Torres (2018).

References—(1) Stassun et al. (2018b), (2) van Leeuwen (2007), (3) Houk & Smith-Moore (1988), (4) Campante et al. (2017), (5) Gaia Collaboration et al. (2018), (6) this work.

Table 2. Stellar Parameters (HD 203949)

Parameter	Value	Source
Basic Properties		
TIC	129649472	1
Hipparcos ID	105854	2
TESS Mag.	4.753	1
Sp. Type	K2 III	3
Spectroscopy		
$T_{\rm eff}$ (K)	4618 ± 113	4
[Fe/H] (dex)	0.17 ± 0.07	4
[α/Fe] (dex)	0.07 ± 0.09	5
$\log g_{\rm spec}$ (cgs)	2.36 ± 0.28	4
SED & *Gaia* DR2 Parallax		
π (mas)	12.7716 ± 0.1239[a]	6
$R_{*,\rm SED}$ ($R_\odot$)	10.30 ± 0.51	5
L_* ($L_\odot$)	43.34 ± 4.27	5
Asteroseismology		
M_* ($M_\odot$)	1.00 ± 0.16	5
R_* ($R_\odot$)	10.34 ± 0.55	5
ρ_* (gcc)	0.00130 ± 0.00011	5
$\log g$ (cgs)	2.415 ± 0.044	5
t (Gyr)	7.29 ± 3.06	5
$\Delta\nu$ (μHz)	4.10 ± 0.14	5
$\nu_{\rm max}$ (μHz)	31.6 ± 3.2	5
$\Delta\Pi_1$ (s)	...	...

[a] Adjusted for the systematic offset of Stassun & Torres (2018).

References—(1) Stassun et al. (2018b), (2) van Leeuwen (2007), (3) Houk (1982), (4) Sousa et al. (2018), (5) this work, (6) Gaia Collaboration et al. (2018).

4. ESTIMATION OF FUNDAMENTAL STELLAR PROPERTIES

Fundamental stellar properties can be estimated by comparing global asteroseismic parameters as well as complementary spectroscopic and astrometric data to the outputs of stellar evolutionary models. We used a number of independent grid-based pipelines in this work (Stello et al. 2009; Basu et al. 2010, 2012; Metcalfe et al. 2010; Gai et al. 2011; Rodrigues et al. 2014, 2017; Silva Aguirre et al. 2015; Yıldız et al. 2016; Serenelli et al. 2017), whereby observables are matched to well-sampled grids of stellar evolutionary tracks. The diversity of grids and optimization procedures employed implicitly account for the impact of using different stellar models — covering a range of input physics — and analysis methodologies on the the final estimates. The adopted set of observables consists of $\{\Delta\nu$, $\nu_{\rm max}$, [Fe/H], $T_{\rm eff}$, $L_*\}$. Given the negligible α enhancement (see Tables 1 and 2), we have therefore ignored its effect.

We provide consolidated values from grid-based modeling for the stellar mass, M_*, radius, R_*, mean density, ρ_*, surface gravity, $\log g$, and age, t, in Tables 1 and 2. To properly account for systematics, values returned by the several pipelines were subject to the same procedure as described in Sect. 3.1 (i.e., single source/method), except that no preliminary outlier rejection step has

Table 3. Mixed-Mode Pattern of HD 212771

$n_{\rm p}$	ℓ	m	$n_{\rm m}$	ζ	$f_{\rm as}$ (μHz)	$f_{\rm obs}$ (μHz)	h
11	1	1	−45	0.718	210.84	210.67	8.1
12	1	1	−41	0.934	223.49	223.34	6.2
12	1	−1	−40	0.775	226.58	226.62	8.2
12	1	1	−40	0.680	227.16	227.27	12.1
12	1	−1	−39	0.441	228.94	228.94	7.6
12	1	−1	−38	0.884	232.08	232.21	5.9
12	1	1	−38	0.910	232.80	232.86	5.8
13	1	−1	−36	0.901	241.01	240.98	10.1
13	1	−1	−35	0.445	244.61	244.43	7.5
13	1	1	−35	0.394	244.95	244.93	11.7
13	1	−1	−34	0.724	247.13	247.05	9.9
13	1	1	−34	0.802	247.74	247.68	5.1
14	1	−1	−31	0.444	261.14	261.20	13.4

NOTE—Each dipole ($\ell = 1$) mixed mode is labeled according to its pressure radial order, $n_{\rm p}$, azimuthal order, m, mixed-mode order, $n_{\rm m}$, and ζ coefficient. The asymptotic guess frequency, $f_{\rm as}$, is given, as well as the observed frequency, $f_{\rm obs}$, and heigh-to-background ratio, h.

now been applied. For completeness, the statistical and systematic errors are $M_* = 1.42 \pm 0.06\,(\rm stat) \pm 0.05\,(\rm sys)\,M_\odot$, $R_* = 4.61 \pm 0.07\,(\rm stat) \pm 0.06\,(\rm sys)\,R_\odot$, $\rho_* = 0.02048 \pm 0.00042\,(\rm stat) \pm 0.00029\,(\rm sys)\ g\,cm^{-3}$, $\log g = 3.263 \pm 0.009\,(\rm stat) \pm 0.005\,(\rm sys)$, and $t = 2.90 \pm 0.25\,(\rm stat) \pm 0.39\,(\rm sys)$ Gyr for HD 212771 and $M_* = 1.00 \pm 0.13\,(\rm stat) \pm 0.09\,(\rm sys)\,M_\odot$, $R_* = 10.34 \pm 0.47\,(\rm stat) \pm 0.29\,(\rm sys)\,R_\odot$, $\rho_* = 0.00130 \pm 0.00009\,(\rm stat) \pm 0.00007\,(\rm sys)\ g\,cm^{-3}$, $\log g = 2.415 \pm 0.030\,(\rm stat) \pm 0.033\,(\rm sys)$, and $t = 7.29 \pm 2.26\,(\rm stat) \pm 2.07\,(\rm sys)$ Gyr for HD 203949.

The properties estimated for HD 212771 in this work are fully consistent with those estimated by Campante et al. (2017) based on K2 asteroseismology. As noted by those authors, the derived asteroseismic mass places HD 212771 in the *retired A star* category[4], being significantly larger than the value reported in the discovery paper (see also North et al. 2017).

Regarding HD 203949, we note the large discrepancy between the asteroseismic mass derived in this work and the mass ($M_* = 2.1 \pm 0.1\,M_\odot$) quoted in the discovery paper, which calls for a revision of both the planet's semimajor axis and minimum mass. We find that $a = 0.63 \pm 0.04$au and $M_{\rm p} \sin i = 5.0 \pm 0.6\,M_{\rm J}$ by assuming an RV semi-amplitude of $178.1 \pm 10.0\,{\rm m\,s^{-1}}$ and an orbital period of 184.2 ± 0.5 days.

The large mass determination in Jones et al. (2014) can, to a large extent, be ascribed to the surface gravity adopted in that work, $\log g = 2.94 \pm 0.20$, consistent with stars in the secondary clump and hence masses $\gtrsim 2\,M_\odot$. Conversely, the lower seismic gravity (see Table 2) is consistent with that of a typical clump star, ruling out a large mass for HD 203949. We stress here that asteroseismology can be used to accurately and robustly determine surface gravities for red giants, with systematic offsets of only a few percent (Pinsonneault et al. 2018).

Finally, we note that the ages of stars in the clump reflect the initial stellar mass and are therefore dependent on the amount of mass loss assumed in the stellar models, which occurs predominantly in the higher RGB. The age quoted in Table 2 corresponds to stellar models based on a Reimers's mass-loss coefficient of $\eta = 0.4$ and an initial mass of $1.2\,M_\odot$. In case a more moderate value is adopted, e.g., $\eta = 0.2$, as suggested by some studies (e.g., Miglio et al. 2012), the age would be centered around 8.9 Gyr, well within uncertainties and corresponding to an initial stellar mass of $1.12\,M_\odot$.

5. DISCUSSION

5.1. *Asteroseismic Performance: TESS vs. Kepler/K2*

HD 212771 was observed by K2 in short cadence (Campante et al. 2017; North et al. 2017), which enabled its asteroseismic investigation. Here, we compare the asteroseismic performances of K2 and TESS by assessing the ratio of the observed maximum oscillation amplitudes for this star, i.e., $A_{\rm max}^{\rm TESS}/A_{\rm max}^{\rm K2}$.

The absolute calibration of the oscillation amplitudes depends on the instrument's bandpass. TESS has a redder bandpass than *Kepler*/K2, meaning observed amplitudes are expected to be lower in the TESS data by a factor of ~ 0.85 (Campante et al. 2016b). We measured the maximum oscillation amplitude per radial mode, $A_{\rm max}$, following the method introduced by Kjeldsen et al. (2005, 2008), which involves determining the peak of the heavily smoothed, background-corrected amplitude oscillation envelope having corrected for the (bandpass-dependent) effective number of modes per radial order[5]. This yielded $A_{\rm max}^{\rm TESS} = 12.8 \pm 2.3$ ppm and $A_{\rm max}^{\rm K2} = 17.1 \pm$

[4] RV planet surveys rely on evolved stars for a sample of intermediate-mass stars (so-called retired A stars), which are more amenable to RV observations than their main-sequence counterparts. However, it has been hypothesized that the masses of subgiant and LLRGB stars targeted by these surveys — typically derived from a combination of spectroscopy and isochrone fitting – may be systematically overestimated (Lloyd 2011).

[5] We used the same K2 light curve as in Campante et al. (2017) in our analysis. We adopted the same background model in the fit to both PSDs.

0.9 ppm, resulting in a ratio $A_{\rm max}^{\rm TESS}/A_{\rm max}^{\rm K2} = 0.75 \pm 0.14$, consistent with the expected ratio.

We caution the reader that the estimated $A_{\rm max}^{\rm TESS}/A_{\rm max}^{\rm K2}$ is prone to unaccounted biases (e.g., Arentoft et al. 2019) arising from the choice of background model and the stochastic nature of the oscillations (coupled to the short time coverage compared to the lifetime of the modes and to the non-contemporaneity of the TESS and K2 datasets). Nevertheless, this preliminary, single-point estimate of $A_{\rm max}^{\rm TESS}/A_{\rm max}^{\rm K2}$ comes in support of the predicted yield of solar-like oscillators using TESS's 2-minute cadence observations (Schofield et al. 2019).

5.2. *HD 203949 b's Orbital Evolution: Avoiding engulfment at the tip of the RGB*

HD 203949 b is one of the few planets which has been observed orbiting a post-RGB star, and hence represents an important window into the life cycle of planetary systems. Most other known planets in this category orbit white dwarfs (Vanderburg et al. 2015; Manser et al. 2019) or pulsars (Wolszczan & Frail 1992; Wolszczan 1994; Sigurdsson et al. 2003), emphasizing the need to place better constraints on planetary evolution during the later giant-branch phases of evolution. HD 203949 b provides us with such an opportunity.

The size, luminosity and mass variations of giant-branch stars often have destructive consequences for planetary systems (Veras 2016). Most prevalent for HD 203949 b is the size variation of the host star, which could incite star-planet tides that may engulf the planet (Villaver & Livio 2009; Kunitomo et al. 2011; Mustill & Villaver 2012; Adams & Bloch 2013; Nordhaus & Spiegel 2013; Valsecchi & Rasio 2014; Villaver et al. 2014; Madappatt et al. 2016; Staff et al. 2016; Gallet et al. 2017; Rao et al. 2018). Both the originally reported stellar mass of $2.1 \pm 0.1\,{\rm M}_\odot$ (Jones et al. 2014) and the asteroseismic stellar mass of $1.00 \pm 0.16\,{\rm M}_\odot$ reported here would tidally influence and probably engulf a Jovian planet on a 184-day orbit at the tip of the RGB.

A planet which is engulfed in the low-density atmosphere of a giant-branch star usually decays quickly enough for it to be considered destroyed. Figure 4 of MacLeod et al. (2018) estimates decay times of engulfed Jovian planets across the Hertzsprung–Russell diagram, and finds that the spiral-in process lasts $\sim 10^0$–10^4 orbits. The upper bound of this range (corresponding to about 5000 yr in our case) is much less than the timescale (about 2 Myr) in which this star's radius exceeds a (0.63 au) during the RGB phase. Hence, HD 203949 b is unlikely to have been engulfed and survive.

Now let us assume that the planet avoided being engulfed. In general, there are two outcomes: (1) the outward expansion of the planet's orbit due to stellar mass loss dominates over tidal effects, and the planet's final semimajor axis increases, or (2) tidal effects dominate over mass loss, but only for a short enough time to prevent engulfment, leading to a decrease in the final semimajor axis. Outcome (2) rarely occurs because the engulfment timescale is so small. Nevertheless, this outcome may explain the current orbit of HD 203949 b.

We explore this possibility by performing numerical simulations of star-planet tides, with the intention of providing rough estimates[6]. We use four different stellar tracks with different values of η, [Fe/H] and atmospheric type (Krishna Swamy and Eddington, which lead to different model $T_{\rm eff}$ scales on the RGB and hence different stellar radii), which fit the currently measured stellar observables. In all cases, a planetary semimajor axis corresponding to a 184-day period (0.63 au) is well within the maximal radial extent of the RGB star, which ranges from 0.85–0.99 au across the four tracks. Therefore, outcome (2) from above applies to this system.

The extent to which the planet was dragged inward changes depending on the details of the tidal formalism adopted. We use a basic formulation of dynamical tides from Zahn (1977) as implemented in Villaver et al. (2014) by (i) including frictional forces from the stellar envelope, (ii) adopting velocity and density prescriptions from eqs. (53) and (54) of Veras et al. (2015), (iii) assuming zero eccentricity throughout the simulation, (iv) assuming a planetary radius of $1.0\,R_{\rm J}$, and (v) assuming adiabatic stellar mass loss, which is a robust approximation for this system (Veras et al. 2011).

In order for the planet to achieve an orbit with a semimajor axis of 0.6–1.0 au, we hence find that the main-sequence semimajor axis of the planet must have resided within an extremely narrow range (an interval much smaller than 10^{-2} au) centered on a specific value within the interval 3.1–3.5 au (which is set by the stellar model adopted and details of the tidal prescription). This result makes sense in the context of, for example, figs. 1, 4 and 6 of Villaver et al. (2014). The probability of finding a planet within such a specific main-sequence semimajor axis range is very low, given that we know of the order of 10^2 planets orbiting giant stars.

A different, perhaps more viable explanation for the current 0.63 au orbit of this planet is that it was gravitationally scattered into its current position after the host

[6] Not considered here are the effects of evaporation of the planet's atmosphere due to the RGB stellar luminosity.

star reached the tip of the RGB[7]. Although RGB mass loss may have triggered the instability which led to this scenario (Debes & Sigurdsson 2002; Veras et al. 2013), more recent suites of simulations of multiple giant-planet systems demonstrate that usually post-mass-loss scattering events — at least for single stars[8] — are delayed until the white dwarf phase (Mustill et al. 2014, 2018; Veras & Gänsicke 2015; Veras et al. 2016, 2018). Therefore, this scattering possibility is also unlikely, but more feasible than the inward tidal drag scenario. Increasing the feasibility is that those scattering studies adopted more massive stars than HD 203949, and hence harbored shorter giant-branch lifetimes in which scattering could occur.

6. OUTLOOK

Characterization of host stars is a critical component of understanding the planets that are hosted by them. For example, the radius of the star is required to estimate the radius of the planet, and the luminosity and effective temperature of the star are crucial ingredients for determining the incident flux received by the planet and the extent of the Habitable Zone (Kane et al. 2016). For known systems observed with TESS, the combination of precision photometry with asteroseismology analysis will aid in the assessment of potential transit events for RV planets (Dalba et al. 2019). Dynamical studies of planetary systems require detailed knowledge of the stellar properties, such as the stellar mass (Menou & Tabachnik 2003). Furthermore, the evolution of orbits as stars move off the main sequence depends on the stellar mass and radius, as these relate to the mass loss relative to the progenitor (Damiani & Mathis 2018). Additionally, the angular size of the host star will be invaluable information when considering known systems as potential direct imaging targets (Kane et al. 2018). Finally, accurate stellar radii for evolved stars will greatly improve the transit probability estimates for the planets, which tend to have the largest probabilities since these scale linearly with stellar radius (Kane et al. 2010). The asteroseismology techniques described here are thus an important component of overall planetary system characterization.

This paper includes data collected by the TESS mission. Funding for the TESS mission is provided by the NASA Explorer Program. Funding for the TESS Asteroseismic Science Operations Center is provided by the Danish National Research Foundation (Grant agreement no.: DNRF106), ESA PRODEX (PEA 4000119301) and Stellar Astrophysics Centre (SAC) at Aarhus University. The project leading to this publication has received funding from the European Union's Horizon 2020 research and innovation programme under the Marie Skłodowska-Curie grant agreement No. 792848 (PULSATION). This work was supported by FCT/MCTES through national funds (UID/FIS/04434/2019). This work was supported by FCT through national funds (PTDC/FIS-AST/30389/2017) and by FEDER through COMPETE2020 (POCI-01-0145-FEDER-030389). This research was supported by the National Science Foundation under Grant No. NSF PHY-1748958 through the Kavli Institute for Theoretical Physics program "Better Stars, Better Planets". M.N.L. acknowledges support from the ESA PRODEX programme. A.S. is partially supported by grants ESP2017-82674-R (Spanish Government) and 2017-SGR-1131 (Generalitat de Catalunya). D.V. gratefully acknowledges the support of the STFC via an Ernest Rutherford Fellowship (grant ST/P003850/1).

Facilities: TESS, *Gaia*, *Kepler*(K2), VLT:Kueyen(UVES), Max Planck:2.2m(FEROS)

Software: TASOC photometry pipeline (https://github.com/tasoc)

REFERENCES

Adams, F. C., & Bloch, A. M. 2013, ApJ, 777, L30, doi: 10.1088/2041-8205/777/2/L30

Adibekyan, V., Figueira, P., Santos, N. C., et al. 2015a, A&A, 583, A94, doi: 10.1051/0004-6361/201527120

Adibekyan, V. Z., Sousa, S. G., Santos, N. C., et al. 2012, A&A, 545, A32, doi: 10.1051/0004-6361/201219401

Adibekyan, V. Z., Benamati, L., Santos, N. C., et al. 2015b, MNRAS, 450, 1900, doi: 10.1093/mnras/stv716

Arentoft, T., Grundahl, F., White, T. R., et al. 2019, A&A, 622, A190, doi: 10.1051/0004-6361/201834690

Baglin, A., Auvergne, M., Barge, P., et al. 2009, in IAU Symposium, Vol. 253, Transiting Planets, ed. F. Pont, D. Sasselov, & M. J. Holman, 71–81

Ballard, S., Chaplin, W. J., Charbonneau, D., et al. 2014, ApJ, 790, 12, doi: 10.1088/0004-637X/790/1/12

[7] Some tidal circularization might have followed the scattering event, as scattering alone usually excites rather than damps orbital eccentricity.

[8] Jones et al. (2014) did detect a long-term linear trend in the RV residuals, which might be attributed to the presence of a distant stellar companion. However, no constraints were placed on the mass nor orbital period of this putative companion.

Basu, S., Chaplin, W. J., & Elsworth, Y. 2010, ApJ, 710, 1596, doi: 10.1088/0004-637X/710/2/1596
Basu, S., Verner, G. A., Chaplin, W. J., & Elsworth, Y. 2012, ApJ, 746, 76, doi: 10.1088/0004-637X/746/1/76
Belkacem, K., Goupil, M. J., Dupret, M. A., et al. 2011, A&A, 530, A142, doi: 10.1051/0004-6361/201116490
Borucki, W. J., Koch, D., Basri, G., et al. 2010, Science, 327, 977, doi: 10.1126/science.1185402
Brown, T. M., Gilliland, R. L., Noyes, R. W., & Ramsey, L. W. 1991, ApJ, 368, 599, doi: 10.1086/169725
Campante, T. L. 2018, Asteroseismology and Exoplanets: Listening to the Stars and Searching for New Worlds, 49, 55, doi: 10.1007/978-3-319-59315-9_3
Campante, T. L., Santos, N. C., & Monteiro, M. J. P. F. G. 2018, Asteroseismology and Exoplanets: Listening to the Stars and Searching for New Worlds, 49. https://arxiv.org/abs/1709.00645
Campante, T. L., Barclay, T., Swift, J. J., et al. 2015, ApJ, 799, 170, doi: 10.1088/0004-637X/799/2/170
Campante, T. L., Lund, M. N., Kuszlewicz, J. S., et al. 2016a, ApJ, 819, 85, doi: 10.3847/0004-637X/819/1/85
Campante, T. L., Schofield, M., Kuszlewicz, J. S., et al. 2016b, ApJ, 830, 138, doi: 10.3847/0004-637X/830/2/138
Campante, T. L., Veras, D., North, T. S. H., et al. 2017, MNRAS, 469, 1360, doi: 10.1093/mnras/stx876
Chaplin, W. J., & Miglio, A. 2013, ARA&A, 51, 353, doi: 10.1146/annurev-astro-082812-140938
Chaplin, W. J., Sanchis-Ojeda, R., Campante, T. L., et al. 2013, ApJ, 766, 101, doi: 10.1088/0004-637X/766/2/101
Corsaro, E., & De Ridder, J. 2014, A&A, 571, A71, doi: 10.1051/0004-6361/201424181
Corsaro, E., De Ridder, J., & García, R. A. 2015, A&A, 579, A83, doi: 10.1051/0004-6361/201525895
Dalba, P. A., Kane, S. R., Barclay, T., et al. 2019, PASP, 131, 034401, doi: 10.1088/1538-3873/aaf183
Damiani, C., & Mathis, S. 2018, A&A, 618, A90, doi: 10.1051/0004-6361/201732538
Davies, G. R., & Miglio, A. 2016, Astronomische Nachrichten, 337, 774, doi: 10.1002/asna.201612371
Davies, G. R., Silva Aguirre, V., Bedding, T. R., et al. 2016, MNRAS, 456, 2183, doi: 10.1093/mnras/stv2593
Debes, J. H., & Sigurdsson, S. 2002, ApJ, 572, 556, doi: 10.1086/340291
Deheuvels, S., Doğan, G., Goupil, M. J., et al. 2014, A&A, 564, A27, doi: 10.1051/0004-6361/201322779
Gai, N., Basu, S., Chaplin, W. J., & Elsworth, Y. 2011, ApJ, 730, 63, doi: 10.1088/0004-637X/730/2/63
Gaia Collaboration, Brown, A. G. A., Vallenari, A., et al. 2018, A&A, 616, A1, doi: 10.1051/0004-6361/201833051
Gallet, F., Bolmont, E., Mathis, S., Charbonnel, C., & Amard, L. 2017, A&A, 604, A112, doi: 10.1051/0004-6361/201730661
Gould, B. A. 1855, AJ, 4, 81, doi: 10.1086/100480
Goupil, M. J., Mosser, B., Marques, J. P., et al. 2013, A&A, 549, A75, doi: 10.1051/0004-6361/201220266
Handberg, R., & Lund, M. N. 2014, MNRAS, 445, 2698, doi: 10.1093/mnras/stu1823
Handberg, R., & Lund, M. N. 2018, T'DA Data Release Notes - Data Release 3 for TESS Sectors 1 + 2, doi: 10.5281/zenodo.2510028. https://doi.org/10.5281/zenodo.2510028
Hekker, S., Elsworth, Y., De Ridder, J., et al. 2011, A&A, 525, A131, doi: 10.1051/0004-6361/201015185
Hon, M., Stello, D., & Yu, J. 2017, MNRAS, 469, 4578, doi: 10.1093/mnras/stx1174
—. 2018, MNRAS, 476, 3233, doi: 10.1093/mnras/sty483
Houk, N. 1982, Michigan Catalogue of Two-dimensional Spectral Types for the HD Stars. Volume 3, Declinations −40°.0 to −26°.0
Houk, N., & Smith-Moore, M. 1988, Michigan Catalogue of Two-dimensional Spectral Types for the HD Stars. Volume 4, Declinations −26°.0 to −12°.0 (Department of Astronomy, University of Michigan, USA)
Howell, S. B., Sobeck, C., Haas, M., et al. 2014, PASP, 126, 398, doi: 10.1086/676406
Huber, D. 2018, Asteroseismology and Exoplanets: Listening to the Stars and Searching for New Worlds, 49, 119, doi: 10.1007/978-3-319-59315-9_6
Huber, D., Stello, D., Bedding, T. R., et al. 2009, Communications in Asteroseismology, 160, 74. https://arxiv.org/abs/0910.2764
Huber, D., Bedding, T. R., Stello, D., et al. 2011, ApJ, 743, 143, doi: 10.1088/0004-637X/743/2/143
Huber, D., Chaplin, W. J., Christensen-Dalsgaard, J., et al. 2013a, ApJ, 767, 127, doi: 10.1088/0004-637X/767/2/127
Huber, D., Carter, J. A., Barbieri, M., et al. 2013b, Science, 342, 331, doi: 10.1126/science.1242066
Huber, D., Chaplin, W. J., Chontos, A., et al. 2019, arXiv e-prints. https://arxiv.org/abs/1901.01643
Jenkins, J. M., Twicken, J. D., McCauliff, S., et al. 2016, in Proc. SPIE, Vol. 9913, Software and Cyberinfrastructure for Astronomy IV, 99133E
Jofré, E., Petrucci, R., Saffe, C., et al. 2015, A&A, 574, A50, doi: 10.1051/0004-6361/201424474
Johnson, J. A., Howard, A. W., Bowler, B. P., et al. 2010, PASP, 122, 701, doi: 10.1086/653809
Johnson, J. A., Fischer, D. A., Marcy, G. W., et al. 2007, ApJ, 665, 785, doi: 10.1086/519677

Jones, M. I., Jenkins, J. S., Bluhm, P., Rojo, P., & Melo, C. H. F. 2014, A&A, 566, A113, doi: 10.1051/0004-6361/201323345
Jones, M. I., Jenkins, J. S., Rojo, P., & Melo, C. H. F. 2011, A&A, 536, A71, doi: 10.1051/0004-6361/201117887
Kallinger, T., De Ridder, J., Hekker, S., et al. 2014, A&A, 570, A41, doi: 10.1051/0004-6361/201424313
Kamiaka, S., Benomar, O., & Suto, Y. 2018, MNRAS, 479, 391, doi: 10.1093/mnras/sty1358
Kamiaka, S., Benomar, O., Suto, Y., et al. 2019, AJ, 157, 137, doi: 10.3847/1538-3881/ab04a9
Kane, S. R., Meshkat, T., & Turnbull, M. C. 2018, AJ, 156, 267, doi: 10.3847/1538-3881/aae981
Kane, S. R., Reffert, S., Henry, G. W., et al. 2010, ApJ, 720, 1644, doi: 10.1088/0004-637X/720/2/1644
Kane, S. R., Hill, M. L., Kasting, J. F., et al. 2016, ApJ, 830, 1, doi: 10.3847/0004-637X/830/1/1
Kjeldsen, H., & Bedding, T. R. 1995, A&A, 293, 87
Kjeldsen, H., Bedding, T. R., Butler, R. P., et al. 2005, ApJ, 635, 1281, doi: 10.1086/497530
Kjeldsen, H., Bedding, T. R., Arentoft, T., et al. 2008, ApJ, 682, 1370, doi: 10.1086/589142
Kunitomo, M., Ikoma, M., Sato, B., Katsuta, Y., & Ida, S. 2011, ApJ, 737, 66, doi: 10.1088/0004-637X/737/2/66
Kurucz, R. L. 2013, ATLAS12: Opacity sampling model atmosphere program. http://ascl.net/1303.024
Lloyd, J. P. 2011, ApJL, 739, L49, doi: 10.1088/2041-8205/739/2/L49
Lund, M. N., Handberg, R., Davies, G. R., Chaplin, W. J., & Jones, C. D. 2015, ApJ, 806, 30, doi: 10.1088/0004-637X/806/1/30
Lund, M. N., Handberg, R., Kjeldsen, H., Chaplin, W. J., & Christensen-Dalsgaard, J. 2017a, in European Physical Journal Web of Conferences, Vol. 160, European Physical Journal Web of Conferences, 01005
Lund, M. N., Silva Aguirre, V., Davies, G. R., et al. 2017b, ApJ, 835, 172, doi: 10.3847/1538-4357/835/2/172
Lundkvist, M. S., Kjeldsen, H., Albrecht, S., et al. 2016, Nature Communications, 7, 11201, doi: 10.1038/ncomms11201
MacLeod, M., Cantiello, M., & Soares-Furtado, M. 2018, ApJ, 853, L1, doi: 10.3847/2041-8213/aaa5fa
Madappatt, N., De Marco, O., & Villaver, E. 2016, MNRAS, 463, 1040, doi: 10.1093/mnras/stw2025
Manser, C. J., Gänsicke, B. T., Eggl, S., et al. 2019, Science, 364, 66, doi: 10.1126/science.aat5330
Mathur, S., García, R. A., Régulo, C., et al. 2010, A&A, 511, A46, doi: 10.1051/0004-6361/200913266
Menou, K., & Tabachnik, S. 2003, ApJ, 583, 473, doi: 10.1086/345359
Metcalfe, T. S., Monteiro, M. J. P. F. G., Thompson, M. J., et al. 2010, ApJ, 723, 1583, doi: 10.1088/0004-637X/723/2/1583
Miglio, A., Brogaard, K., Stello, D., et al. 2012, MNRAS, 419, 2077, doi: 10.1111/j.1365-2966.2011.19859.x
Mosser, B., & Appourchaux, T. 2009, A&A, 508, 877, doi: 10.1051/0004-6361/200912944
Mosser, B., Gehan, C., Belkacem, K., et al. 2018, A&A, 618, A109, doi: 10.1051/0004-6361/201832777
Mosser, B., Pinçon, C., Belkacem, K., Takata, M., & Vrard, M. 2017, A&A, 600, A1, doi: 10.1051/0004-6361/201630053
Mosser, B., Vrard, M., Belkacem, K., Deheuvels, S., & Goupil, M. J. 2015, A&A, 584, A50, doi: 10.1051/0004-6361/201527075
Mosser, B., Belkacem, K., Goupil, M. J., et al. 2011, A&A, 525, L9, doi: 10.1051/0004-6361/201015440
Mosser, B., Goupil, M. J., Belkacem, K., et al. 2012, A&A, 540, A143, doi: 10.1051/0004-6361/201118519
Mosser, B., Benomar, O., Belkacem, K., et al. 2014, A&A, 572, L5, doi: 10.1051/0004-6361/201425039
Mustill, A. J., Veras, D., & Villaver, E. 2014, MNRAS, 437, 1404, doi: 10.1093/mnras/stt1973
Mustill, A. J., & Villaver, E. 2012, ApJ, 761, 121, doi: 10.1088/0004-637X/761/2/121
Mustill, A. J., Villaver, E., Veras, D., Gänsicke, B. T., & Bonsor, A. 2018, MNRAS, 476, 3939, doi: 10.1093/mnras/sty446
Nordhaus, J., & Spiegel, D. S. 2013, MNRAS, 432, 500, doi: 10.1093/mnras/stt569
North, T. S. H., Campante, T. L., Miglio, A., et al. 2017, MNRAS, 472, 1866, doi: 10.1093/mnras/stx2009
Nsamba, B., Campante, T. L., Monteiro, M. J. P. F. G., et al. 2018, MNRAS, 477, 5052, doi: 10.1093/mnras/sty948
Peirce, B. 1852, AJ, 2, 161, doi: 10.1086/100259
Pinsonneault, M. H., Elsworth, Y. P., Tayar, J., et al. 2018, ApJS, 239, 32, doi: 10.3847/1538-4365/aaebfd
Rao, S., Meynet, G., Eggenberger, P., et al. 2018, A&A, 618, A18, doi: 10.1051/0004-6361/201833107
Rauer, H., Catala, C., Aerts, C., et al. 2014, Experimental Astronomy, 38, 249, doi: 10.1007/s10686-014-9383-4
Rendle, B. M., Buldgen, G., Miglio, A., et al. 2019, MNRAS, 484, 771, doi: 10.1093/mnras/stz031
Ricker, G. R., Winn, J. N., Vanderspek, R., et al. 2015, Journal of Astronomical Telescopes, Instruments, and Systems, 1, 014003, doi: 10.1117/1.JATIS.1.1.014003
Rodrigues, T. S., Girardi, L., Miglio, A., et al. 2014, MNRAS, 445, 2758, doi: 10.1093/mnras/stu1907

Rodrigues, T. S., Bossini, D., Miglio, A., et al. 2017, MNRAS, 467, 1433, doi: 10.1093/mnras/stx120
Santos, N. C., Sousa, S. G., Mortier, A., et al. 2013, A&A, 556, A150, doi: 10.1051/0004-6361/201321286
Schlegel, D. J., Finkbeiner, D. P., & Davis, M. 1998, ApJ, 500, 525, doi: 10.1086/305772
Schofield, M., Chaplin, W. J., Huber, D., et al. 2019, ApJS, 241, 12, doi: 10.3847/1538-4365/ab04f5
Serenelli, A., Johnson, J., Huber, D., et al. 2017, ApJS, 233, 23, doi: 10.3847/1538-4365/aa97df
Sigurdsson, S., Richer, H. B., Hansen, B. M., Stairs, I. H., & Thorsett, S. E. 2003, Science, 301, 193, doi: 10.1126/science.1086326
Silva Aguirre, V., Davies, G. R., Basu, S., et al. 2015, MNRAS, 452, 2127, doi: 10.1093/mnras/stv1388
Silva Aguirre, V., Lund, M. N., Antia, H. M., et al. 2017, ApJ, 835, 173, doi: 10.3847/1538-4357/835/2/173
Sliski, D. H., & Kipping, D. M. 2014, ApJ, 788, 148, doi: 10.1088/0004-637X/788/2/148
Sousa, S. G., Adibekyan, V., Delgado-Mena, E., et al. 2018, A&A, 620, A58, doi: 10.1051/0004-6361/201833350
Staff, J. E., De Marco, O., Wood, P., Galaviz, P., & Passy, J.-C. 2016, MNRAS, 458, 832, doi: 10.1093/mnras/stw331
Stassun, K. G., Corsaro, E., Pepper, J. A., & Gaudi, B. S. 2018a, AJ, 155, 22, doi: 10.3847/1538-3881/aa998a
Stassun, K. G., & Torres, G. 2016, AJ, 152, 180, doi: 10.3847/0004-6256/152/6/180
—. 2018, ApJ, 862, 61, doi: 10.3847/1538-4357/aacafc
Stassun, K. G., Oelkers, R. J., Pepper, J., et al. 2018b, AJ, 156, 102, doi: 10.3847/1538-3881/aad050
Stello, D., Chaplin, W. J., Bruntt, H., et al. 2009, ApJ, 700, 1589, doi: 10.1088/0004-637X/700/2/1589
Stock, S., Reffert, S., & Quirrenbach, A. 2018, A&A, 616, A33, doi: 10.1051/0004-6361/201833111
Valsecchi, F., & Rasio, F. A. 2014, ApJ, 786, 102, doi: 10.1088/0004-637X/786/2/102
Van Eylen, V., & Albrecht, S. 2015, ApJ, 808, 126, doi: 10.1088/0004-637X/808/2/126
Van Eylen, V., Albrecht, S., Huang, X., et al. 2019, AJ, 157, 61, doi: 10.3847/1538-3881/aaf22f
van Leeuwen, F. 2007, A&A, 474, 653, doi: 10.1051/0004-6361:20078357
Vanderburg, A., Johnson, J. A., Rappaport, S., et al. 2015, Nature, 526, 546, doi: 10.1038/nature15527
Veras, D. 2016, Royal Society Open Science, 3, 150571, doi: 10.1098/rsos.150571
Veras, D., Eggl, S., & Gänsicke, B. T. 2015, MNRAS, 451, 2814, doi: 10.1093/mnras/stv1047
Veras, D., & Gänsicke, B. T. 2015, MNRAS, 447, 1049, doi: 10.1093/mnras/stu2475
Veras, D., Georgakarakos, N., Gänsicke, B. T., & Dobbs-Dixon, I. 2018, MNRAS, 481, 2180, doi: 10.1093/mnras/sty2409
Veras, D., Mustill, A. J., Bonsor, A., & Wyatt, M. C. 2013, MNRAS, 431, 1686, doi: 10.1093/mnras/stt289
Veras, D., Mustill, A. J., Gänsicke, B. T., et al. 2016, MNRAS, 458, 3942, doi: 10.1093/mnras/stw476
Veras, D., Wyatt, M. C., Mustill, A. J., Bonsor, A., & Eldridge, J. J. 2011, MNRAS, 417, 2104, doi: 10.1111/j.1365-2966.2011.19393.x
Verner, G. A., Elsworth, Y., Chaplin, W. J., et al. 2011, MNRAS, 415, 3539, doi: 10.1111/j.1365-2966.2011.18968.x
Villaver, E., & Livio, M. 2009, ApJ, 705, L81, doi: 10.1088/0004-637X/705/1/L81
Villaver, E., Livio, M., Mustill, A. J., & Siess, L. 2014, ApJ, 794, 3, doi: 10.1088/0004-637X/794/1/3
Vrard, M., Mosser, B., & Samadi, R. 2016, A&A, 588, A87, doi: 10.1051/0004-6361/201527259
Wolszczan, A. 1994, Science, 264, 538, doi: 10.1126/science.264.5158.538
Wolszczan, A., & Frail, D. A. 1992, Nature, 355, 145, doi: 10.1038/355145a0
Yıldız, M., Çelik Orhan, Z., & Kayhan, C. 2016, MNRAS, 462, 1577, doi: 10.1093/mnras/stw1709
Yu, J., Huber, D., Bedding, T. R., et al. 2018, ApJS, 236, 42, doi: 10.3847/1538-4365/aaaf74
Zahn, J. P. 1977, A&A, 500, 121